# Thermal stability of atmospheric plasma sprayed (Ni, Cu, Co)-YSZ and Ni-Cu-Co-YSZ anodes cermets for SOFC application

Amel Benyoucef, Didier Klein, Olivier Rapaud, Christian Coddet, Boumediene Benyoucef

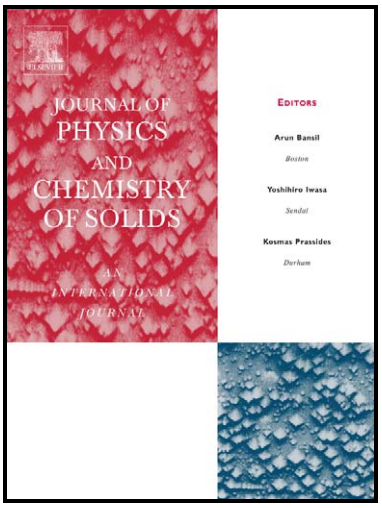


www.elsevier.com/locate/jpcs

# Thermal stability of atmospheric plasma sprayed (Ni, Cu, Co)-YSZ and Ni-Cu-Co-YSZ anodes cermets for SOFC application

Amel Benyoucef, Didier Klein, Olivier Rapaud, Christian Coddet, Boumediene Benyoucef

PII: S0022-3697(09)00264-9
DOI: doi:10.1016/j.jpcs.2009.09.009
Reference: PCS 5947

To appear in: *Journal of Physics and Chemistry of Solids*

Received date: 13 April 2009
Revised date: 10 September 2009
Accepted date: 15 September 2009

Cite this article as: Amel Benyoucef, Didier Klein, Olivier Rapaud, Christian Coddet and Boumediene Benyoucef, Thermal stability of atmospheric plasma sprayed (Ni, Cu, Co)-YSZ and Ni-Cu-Co-YSZ anodes cermets for SOFC application, *Journal of Physics and Chemistry of Solids*, doi:10.1016/j.jpcs.2009.09.009

# Thermal stability of atmospheric plasma sprayed (Ni, Cu, Co)-YSZ and Ni-Cu-Co-YSZ anodes cermets for SOFC application.

Amel Benyoucef [(1)*], Didier Klein[(1)] , Olivier Rapaud[(1)], Christian Coddet[(1)] , Boumediene Benyoucef [(2)]

[1] Laboratoire d'Etudes et de Recherches sur les Matériaux, les Procédés et les Surfaces, Université de Technologie de Belfort-Montbéliard, Site de Montbéliard, 90010 Belfort cedex, France.

[2] Unité de Recherche Matériaux et Energies Renouvelables, Université Abou-bakr Belkaïd de Tlemcen, 13000, Tlemcen, Algérie.

* Corresponding author. E-mail address: amel.benyoucef@utbm.fr, Phone: 33 (0)3 84 58 37 30, Fax: 33 (0) 3 84 58 37 37



**Abstract**

This paper reports the results of the thermal stability study of M-YSZ (M= Ni, Cu, Co, Cu-Co, Ni-Cu-Co) SOFC anode cermets materials at different heat treatment temperatures. The cermets were elaborated by atmospheric plasma spraying (APS) with optimised conditions and then submitted to heat treatments at 800°C and 1000°C, respectively. Scanning electron microscopy and X-ray diffraction were used to characterise, respectively, the morphology and structure of obtained films, before and after thermal annealing. A correlation was made between the differential scanning calorimetry analysis results and those obtained by X-ray diffraction. Focusing, in this study, on YSZ matrix thermal stability, the obtained results were as following: the

monometallic cermets with the lowest amount of metal and the trimetallic one, exhibited a good stability at 800°C whereas at 1000°C, all considered cermets, were unstable with an eutectoid decomposition of YSZ matrix.

**Keywords:** A. ceramics, A. metals, B. plasma deposition, C. X-ray diffraction, C. Differential scanning calorimetry (DSC).

## 1. Introduction

Cubic Yttria stabilised Zirconia ($(Y_2O_3)_{0.08}$-$(ZrO_2)_{0.92}$ abbreviated as YSZ) is offering a good chemical stability and a high ionic conductivity, at elevated operating temperatures ~1000°C. This leads to its wide utilization in anode cermets for Solid Oxide Fuel Cells [1-4]. However, to submit YSZ cubic phase to high temperatures ~1000°C, induces a significant drop in conductivity. This phenomenon was correlated by the authors, with the allotropic transformations that occur in the ceramic matrix when subjected to such temperatures [5-9]. In fact, many works on fully stabilized zirconia have shown that once subjected to 900°C - 1000°C range of thermal cycling temperatures, the slow cooling of this cubic phase leaded to the emergence of new allotropic forms following an eutectoid decomposition in the vicinity of 600°C, namely cubic form and tetragonal one which in turn is transformed into monoclinic phase since it cooled very slowly [7, 9-12].

So, in this present work, we propose to study the thermal behaviour and affects on the crystalline phase stability of the YSZ ceramic matrix of different anode cermets, after heat treatments at 800°C and 1000°C, respectively. Elements like Ni, Cu, Co are good conductors and also, possess excellent catalytic activity for $CH_4$ activation and

combustion [13, 14] that is why M-YSZ (M= Ni, Cu, Co, Cu-Co, Ni-Cu-Co) are studied here as potential SOFC anode materials running directly on $CH_4$. These coatings were elaborated by atmospheric plasma spraying (APS) technique. Many processes were developed for SOFCs anode cermets achievement, among them, the conventional ceramic sintering, a low cost solid-state method and an easy one to realize [15-19]. However, APS which is a plasma based method, is still being the most advantageous one because it does not require subsequent heat treatment, leading thus to a more faster method than the conventional one and a less expensive one for SOFCs components achievement [20-23], comparing with others deposition processes such as electrochemical vapour deposition [24] and vacuum plasma spray [25], which need sophisticated equipments and a controlled atmosphere that consequently increases the fabrication cost. Moreover, APS easily controls the microstructure and material deposition rates through variation of spray parameters [26].



## 2. Experimental

The M-YSZ (M= Ni, Cu, Co, Cu-Co, Ni-Cu-Co) different coatings were elaborated by Atmospheric Plasma Spraying (APS) of their respective feedstock powders, with optimized conditions listed in Table 1. The plasma spraying was carried out using a Sulzer-Metco Pt-2000 F4MB torch for APS, assembled on ABB robot arm. Two means of cooling were used jointly: compressed air blasts placed each side of the torch and two tubes Venturi behind the substrate. Feedstock powders are a mixture of metals Ni, Cu, Co and yttria stabilized zirconia (8% mol YSZ). For monometallic cermets materials Ni-YSZ, Cu-YSZ and Co-YSZ respectively, weight ratios are successively (2:3), (1:1) and (3:2). The Cu-Co-YSZ bimetallic and Ni-Cu-Co-YSZ trimetallic cermets materials are in (0.5:1:2.5) and (1:1:1:2) weight ratios respectively.

All details about feedstock powders preparation and optimization of thermal spraying conditions, to spray a gas-permeable anode coating as porous as possible, were given in a previous work [27].

The X-ray diffraction (carried on D8 Focus Bruker AXS with Co Kα radiation λ=1.7889 Å) and Scanning Electron Microscopy (JEOL JSM-5800LV, 25 keV) were used to characterize respectively the structure and morphology of coatings achieved with the optimized parameters.

All considered coatings, were subjected to heat treatments at 800°C and 1000°C in air ambience for 1 hour with a heating rate of 10°C/min. After a slow cooling in closed furnace, these coatings were submitted to X-ray diffraction analysis. The obtained results were then correlated with those of the simultaneous Thermogravimetry - Differential Scanning Calorimetry (TG-DSC) analysis. The thermal analysis was performed on a JUPITER (NETZSCH) STA 449C unit equipped with a very high temperature (till 1650°C) furnace and an accuracy microbalance (max: 5g, resolution 0.1µg). Measurements took place from room temperature to 1150°C with a heating rate of 10°C/min. The same analysing conditions were maintained for all coatings to note dynamic mode under $N_2$ flow rate (60 ml/min).



**3. Results and Discussion**

The feedstock powders were sprayed with the optimized parameters listed in table 1. The following combination of superior spray distance, minor argon flow rate, middle carrying gas flow rate and the highest hydrogen flow rate yielded a decrease in both particle velocity and temperature and leaded to M-YSZ (M= Ni, Cu, Co, Cu-Co, Ni-Cu-Co) porous anode coatings with thicknesses of about 200 µm and an average porosity of 19 % measured by statistical SEM cross-sectional images analysis.

3.1 Morphology of elaborated coatings

The scanning electron microscopy (SEM) characterization of the obtained M-YSZ (M= Ni, Cu, Co, Cu-Co, Ni-Cu-Co) coatings leaded to very similar results in term of coating morphology, a characteristic one of atmospheric plasma sprayed materials, namely a rough surface as it is shown in Fig. 1 (a) and (b) for Ni-YSZ (2:3) and Ni-Cu-Co-YSZ (1:1:1:2) respectively and a bimodal structure: unmelted zones and fully melted ones with a porous lamellar microstructure including coarse and planar pores as it is given by the images of the cross-sectional microstructures in Fig. 2 (a) and (b) for Ni-YSZ (2:3) and Ni-Cu-Co-YSZ (1:1:1:2), respectively and fracture profiles in Fig. 3 (a) and (b) for Cu-YSZ (2:3) and Co-YSZ (2:3), respectively. In fact, in this kind of cermets elaborating process, when the supplied powders are sprayed, they are firstly melted and then propelled, to reach the substrate with assuming spherical shape during their flight due to the surface tension, but they will be considerably deformed at impingement on the substrate, losing their kinetic and thermal energy and then, will solidify in lamellas forms at a cooling rate of $10^6$ $K.s^{-1}$ [28]. The succession of impacts of powder particles, which are fully or partially melted, creates a superposition of irregular lamellas, leading to a bimodal structure, also known as composite structure, with the coexistence of a porous area and another one in the form of clusters of grains [29-32]. It can be seen, in Fig. 3, that some deposited lamellas have a columnar structure within the splat due to the molten particles rapid solidification process. These lamellas are of about 2-3 µm, 4-5 µm thick for Cu-YSZ (2:3) and Co-YSZ (2:3) coatings respectively, with 1-2 splat layers, of about 1 µm a thickness, in each one.

3.2 Crystalline structure of elaborated coatings

3.2.1 Before heat treatment

The XRD patterns for Ni-YSZ (2:3), Cu-YSZ (2:3), Co-YSZ (2:3), Cu-Co-YSZ (0.5:1:2.5) and Ni-Cu-Co-YSZ (1:1:1:2) coatings achieved with the optimized parameters, are shown in Fig. 4. So, it can be seen that the characteristic peaks of YSZ ceramic matrix in its cubic phase, namely YSZ (111) at 2θ =35.081°, are revealed for all coatings. Otherwise, Ni-YSZ and Co-YSZ monometallic coatings were containing Ni and Co crystalline phases, respectively, with their characteristic peaks Ni (111) at 2θ =52.178° and Co (111) at 2θ =51.830° and a few amount of oxides forms NiO and CoO, respectively, due to atmospheric spraying high temperature. For cobalt case, there are two known stable oxides CoO and $Co_3O_4$ but CoO is thermodynamically stable at temperatures above 900 °C, whereas $Co_3O_4$ is formed at lower temperatures, even both oxide forms are kinetically stable at room temperature [33]. So, APS high temperature process leads to CoO oxide formation preferentially.

The Cu-YSZ coating revealed Cu crystalline phase Cu (111) at 2θ =50.731° with a very small residue of $Cu_2O$ phase. This oxide was precipitated on cubic lattice which is the most stable one at high temperatures. In fact, at above 800°C, copper oxidation under ambient oxygen pressures has been extensively studied [34-36] and it appears that only $Cu_2O$ is thermodynamically stable and that CuO with monoclinic lattice could not be formed, if oxygen pressure is not above the dissociation pressure of CuO.

For Cu-Co-YSZ bimetallic coating, the XRD pattern revealed the characteristic peaks of Cu and Co, respectively and showed that CoO (200) and $Cu_2O$ (111) oxides, with their respective characteristic peaks at 2θ = 49.645° and 2θ = 49.645°, were both existing. The presence of these oxides is justified by the coating elaborating process. They both precipitate in a cubic phase, with very close lattice parameters, a = 4.2612 Å and a = 4.2696 Å, respectively, which means that there must be an overlap between the corresponding characteristic peaks positions. That is why we have chosen to index the

two oxides simultaneously on the same peak, knowing that both were indeed present if one refers to what has been obtained for Cu-YSZ and Co-YSZ monometallic cermets, which were elaborated in the same APS conditions.

The XRD pattern of Ni-Cu-Co-YSZ coating revealed the characteristic peaks of Cu, NiO, CoO and $Cu_2O$ crystalline phases with sill an overlap between CoO and $Cu_2O$ characteristic peaks. However, for Ni (111) at 2θ =52.178° and Co (111) at 2θ =51.830° elements, their respective characteristic peaks are not discernable. This could be due partly to the fact that, during the thermal spraying process, Ni and Co are solidified in the same crystalline structure (CFC) with very close respective lattice parameters a = 3.5238 Å and a = 3.5447 Å and in an other hand, to the possibility that have these two metals, completely miscible in one another to form a solid solution [37] during the spraying process, which makes their identification separately impossible.

It is necessary to precise that according to the obtained XRD results for these three kinds of monometallic cermets, the percentages of metals in the cermets had a negligible influence on crystalline phase structures and it was only intensities of principal peaks that changed.

3.2.2 After heat treatment

XRD patterns of Ni-YSZ (2:3), Cu-YSZ (2:3) and Co-YSZ (2:3) after heat treatments at 800°C and 1000°C in air ambiance are given in Figs. 5, 6 and 7, respectively. We can see that for all types of monometallic cermets, heat treatments at 800°C and 1000°C induced a significant metal oxidation with a complete disappearance of metallic forms at 1000°C and the appearance of the characteristic peaks of NiO, CuO and $Co_3O_4$ oxides, respectively, for Ni-YSZ, Cu-YSZ and Co-YSZ coatings. Furthermore, for the three kinds of cermets, there was no effect of heat treatment at 800°C on the YSZ matrix structure stability, in contrast to 1000°C where the emergence

of new crystalline phases were observed, cubic $Y_2O_3$ with (111) characteristic peak at $2\theta = 34.287°$ and $ZrO_2$ monoclinic form with the characteristic peak (-111) at $2\theta = 32.836°$. This result is due to the YSZ eutectoid decomposition that occurs during cermets slow cooling (closed furnace) leading thus to the transformation of cubic YSZ in a mixture of cubic phase and tetragonal phase that rose then to the monoclinic form with $Y_2O_3$ precipitation [7, 9-12 ].

So, when we have seen that (2:3) M-YSZ (M= Ni, Cu, Co) monometallic cermets were stable at 800°C, we have chosen to submit the others (1:1) and (3:2) cermets to heat treatment under the same conditions of temperature in order to study the effect of metal proportion in the cermet on the YSZ ceramic matrix stability. Fig. 8 shows the XRD patterns of Cu-YSZ at different weight ratios (2:3), (1:1) and (3:2) after heat treatment at 800°C/ 1 hour in air ambiance. So, we can see that (3:2) Cu-YSZ is the only one that showed a bad stability at the considered temperature, with an eutectoid decomposition of YSZ. The same results were obtained for (3:2) Ni-YSZ and (3:2) Co-YSZ cermets when submitted to the same conditions of heat treatment. Thus, it appeared that the metal proportion in the cermet was an important factor for its thermal stability. So, the metal amount increase was leading to a decrease of the ceramic matrix stability.

To comfort the XRD result, TG-DSC measurements were achieved for considered Ni-YSZ, Cu-YSZ and Co-YSZ monometallic cermets at their different (2:3), (1:1) and (3:2) weight ratios. Fig. 9 illustrates the obtained results for Cu-YSZ cermets. The TG signals, for the different weight ratios (2:3), (1:1) and (3:2), revealed that there was not any mass loss. However, the DSC signals all showed an endothermic peak at the respective temperatures 1071.6°C, 1072.4°C and 1073.0°C, characterizing the melting point of copper. We will notice that these temperatures that are characterising a well

defined phase change, a solid one to a liquid one, were very close, with an average of ~ 1072.3°C, slightly below that of pure copper melting point (1084.6°C). This could be justified since copper is being dispersed in the ceramic matrix. It should be noted that in term of TG-DSC analysis, metallic copper, was detected at high temperature and was revealed by its melting peak, because the measurements were carried out under flow of nitrogen. This allowed us to confirm that there are no oxidation phenomena in these conditions of analysis. Otherwise, we saw an exothermic transformation, before copper melting point, with maximum temperatures of 847.7°C, 848.0°C and 769.0°C for Cu-YSZ cermets at (2:3), (1:1) and (3:2) proportions, respectively. It can be noted that, except the melting points peaks, Ni-YSZ and Co-YSZ cermets exhibited the same behaviours as those of Cu-YSZ cermets, when submitted to the same TG-DSC analysis conditions. At this stage of investigation, we could not say what type of transformation took place at these temperatures, but nevertheless, there was a relationship between the results obtained by XRD and the TG-DSC analysis. Indeed, it was observed that for both (2:3) and (1:1) M-YSZ cermets proportions, the maximum temperatures, for the occurring exothermic phenomena, were higher than 800°C and consequently greater than those observed for (3:2) M-YSZ cermets, lower temperatures than 800°C. This is describing a thermal instability phenomenon of (3:2) M-YSZ cermets at 800°C. So, trying to explain this phenomenon, we issued a hypothesis, which remains to verified: the maximum temperatures observed for the DSC profiles correspond to those beyond which the cermet starts to become thermally unstable. This corroborated the XRD analysis results, where the heat treatment of (3:2) M-YSZ cermets at 800°C, a higher temperature of those critical for an exothermic transformation, leaded to damage into the ceramic matrix due to the eutectoid decomposition of YSZ matrix.

Fig. 10 reveals that for the Cu-Co-YSZ (0.5:1:2.5) bimetallic cermet, heat treatments at 800°C as well as 1000°C leaded to Cu and Co metals oxidation and the appearance of their respective oxides CuO and $Co_3O_4$ and also leaded to YSZ matrix eutectoid decomposition as listed before with the emergence of new crystalline phases, cubic $Y_2O_3$ and monoclinic $ZrO_2$. The correlation between these results and those obtained by the TG-DSC analysis and given in Fig. 11, is very promising, since an exothermic phenomenon, with a maximum temperature at 606.1°C, had been observed. By adopting the same reasoning as for the other cermets cases, the critical threshold for the thermal stability of this cermet is at about 606.1°C. So, when this cermet is subjected to higher temperatures such 800°C or 1000°C, cubic zirconia loses its stability and undergoes an eutectoid decomposition as described before for monometallic cermets. One endothermic peak was observed at 1114.2°C, probably indicating the copper melting point. It is a temperature slightly higher than that of pure copper melting point, which is justified since Cu and Co coexist in the same cermet leading thus to an increase of Cu melting point. Furthermore, it should be noted that the TG analysis did not reveal any mass loss.

XRD patterns in Fig. 12 show that heat treatment of the Ni-Cu-Co-YSZ (1:1:1:2) trimetallic cermet, at 800°C, leaded to Ni, Cu and Co metals oxidation to their respective NiO, CuO and $Co_3O_4$ oxides, in contrast to 1000°C, where the metallic forms disappeared entirely as well as CuO and $Co_3O_4$ oxides and where it emerged a new crystalline phase characteristic of a CFC $Cu_{0.76}Co_{2.24}O_4$ binary oxide with a (311) preferential orientation at $2\theta = 42.993°$. Furthermore, with regard to the ceramic matrix stability, heat treatment at 1000°C contrary to 800°C induced YSZ eutectoid decomposition revealed by the appearance of $Y_2O_3$ and $ZrO_2$ characteristic peaks. TG-DSC measurements achieved on this cermet are given in Fig. 13. Through the TG signal

analysis, we can see a slight change in mass of about 2% at approximately 400°C which can not be explained at this stage of investigation and then considered negligible for the rest of our interpretation. The DSC analysis revealed a small endothermic peak at ~ 1074.5°C, probably related to copper melting point, preceded by an exothermic phenomenon at ~ 1060.3°C. If we adopt the same reasoning as for the other cermets, this cermet behaviour, observed at 800 ° C, is fully justified; this means that it had not yet reached the threshold temperature of 1060°C, remaining thus cermet stability at 800°C without any eutectoid decomposition of the ceramic matrix.

**4. Conclusion**

Different types of M-YSZ (M= Ni, Cu, Co, Cu-Co, Ni-Cu-Co) cermets, at different weight ratios, were elaborated with the optimized APS parameters which offered the best microstructure and porosity for SOFCs anodic application. The different coatings SEM analysis showed the same morphology, a characteristic one of atmospheric plasma sprayed materials namely a rough surface and a bimodal structure.

The coatings XRD investigations before heat treatment revealed all the characteristic peaks of each kind of metal in the cermet with a presence of their respective oxides that is justified by the coating elaborating process namely air ambiance and a very high temperature. In addition, XRD results showed that, after spraying, the YSZ ceramic matrix of all considered coatings, was obtained in its cubic crystalline phase which is the most sought for SOFCs application due of its ionic conductive property at high temperature. This can be explained by the fact that the cermets APS elaborating process leads to such behaviour, with the freeze of melted materials in their most stable allotropic form, as consequence of their extremely rapid cooling, when they are propelled on the cooled substrate. After heat treatments of the

different considered coatings, at 800°C and 1000°C, the XRD analysis results were correlated to those obtained by TG-DSC measurements. This revealed that all monometallic cermets M-YSZ (M= Ni, Cu and Co) at (2:3) were stable at 800°C and notified that the increase of metal mass proportion in the cermets reduced greatly their thermal stability, such for cermets at (3:2) weight ratio, leading thus to an eutectoid decomposition of the YSZ ceramic matrix during its slow cooling in a closed furnace. We, furthermore, have seen that bimetallic Cu-Co-YSZ cermet presented a bad thermal stability at 800°C and that all kinds of studied cermets were thermally unstable at 1000°C. So, to conclude, monometallic (2:3) M-YSZ cermets (M= Ni, Cu, and Co) and the trimetallic (1:1:1:2) Ni-Cu-Co-YSZ cermet, revealed the most promising characteristics for SOFCs anodic application in term of structure, morphology and thermal stability, at 800°C which is the most common SOFCs operating temperature.

**Acknowledgements**

The authors are indebted to CAPM for its financial support of this study. They also would like to express a sincere gratitude to Sophie Lamy the LERMPS/Université de Technologie de Belfort-Montbéliard, for her collaboration.

**References**

1. N. K. Minh, Ceramic Fuel Cells, J. Amer.Cer. Soc., 76 (3) (1993) 563.

2. J. Kondoh, T. Kawashima, S. Kikuchi, Y. Tomii, Y. Ito, Effect of Aging on Yttria Stabilized Zirconia, J. Electrochem. Soc., 145 (1998) 1527.

3. M.L. Perry, T.F. Fuller, A Historical Perspective of Fuel Cell Technology in the 20th Century, J. Electrochem. Soc., 149 (2002) 59.

4. Hiroki Kondo, Tohru Sekino, Takafumi Kusunose, Tadachika Nakayama, Yo Yamamoto, Koichi Niihara, Phase stability and electrical property of NiO-doped yttria-stabilized zirconia, Materials Letters, 57 (2003) 1624.

5. F.T. Ciacchi, K.M. Crane, S.P.S. Badwal, Solid State Ion., 73 (1994) 49.

6. I.R. Gibson, G.P. Dransfield, J.T.S. Irvine, J. Eur. Ceram. Soc.,18 (1998) 661.

7. Hiroki Kondo, Tohru Sekino, Takafumi Kusunose, Tadachika Nakayama, Yo Yamamoto, Koichi Niihara, Phase stability and electrical property of NiO-doped yttria-stabilized zirconia, Materials Letters, 57 (2003) 1624.

8. Masatoshi Hattori, Yasuo Takeda, Yoshinori Sakaki, Akihiro Nakanishi, Satoshi Ohara, Kazuo Mukai, Jin-Ho Lee, Takehisa Fukui, Effect of aging on conductivity of yttria stabilized zirconia, Journal of Power Sources, 126 (2004) 23.

9. Junya Kondoh, Shiomi Kikuchi, Voichi Tomii, and Yasuhiko Ito, Effect of Aging on Yltria-Stabilized Zirconia, II. A Study of the Effect of the Microsfructure on Conductivity, J. Electrochem. Soc., 145 (5) (1998) 1536.

10. Junya Kondoh, Shiomi Kikuchi, Yoichi Tomii, and Yasuhiko Ito, Effect of Aging on Yttria-Stabilizecl Zirconia, Ill. A Study of the Effect of Local Sfructures on Conductivity, J. Electrochem. Soc., 145 (5) (1998) 1550.

11. K. Nomura, Y. Mizutani , M. Kawai , Y. Nakamura , O. Yamamoto, Aging and Raman scattering study of scandia and yttria doped Zirconia, Solid State Ionics, 132 (2000) 235.

12. Kan Hachiya, Koichi Suzaki, Yoichi Tomii, Junya Kondoh, Aging-induced change of photoluminescence in yttria-fully-stabilized ZrO2 with $Sc_2O_3$ or $In_2O_3$ doping, Electrochimica Acta ,53 (2007) 66.

13. S. McIntosh, J.M. Vohs, R.J. Gorte, Electrochim. Acta , 47 (2002) 3815.

14. R.J. Gorte, S. Park, J.M. Vohs, C.H. Wang, Adv. Mater., 12 (2000) 1465.

15. Xiqiang Huang, Zhiguo Liu, Zhe Lu, Li Pei, Ruibin Zhu, Yuqiang Liu, Jipeng Miao, Zhiguo Zhang, Wenhui Su

, Journal of Physics and Chemistry of Solids 64 (2003) 2379.

16. Lijun Zhao, Xiqiang Huang, Ruibin Zhu, Zhe Lu, Weiwei Sun, Yaohui Zhang, Xiaodong Ge, Zhiguo Liu, Wenhui Su, Journal of Physics and Chemistry of Solids 69 (2008) 2019.

17. Xiqiang Huang, Zhe Lu, Li Pei, Zhiguo Liu, Yuqiang Liu, Ruibin Zhu, Jipeng Miao,

Zhiguo Zhang, Wenhui Su, Journal of Alloys and Compounds 360 (2003) 294.

18. Xiaodong Ge, Xiqiang Huang, Yaohui Zhang, Zhe Lu, Jiahuan Xu, Kongfa Chen, Dawei Dong, Zhiguo Liu, Jipeng Miao, Wenhui Su

, Journal of Power Sources 159 (2006) 1048.

19. Weiwei Sun, Xiqiang Huang, Zhe Lu, Lijun Zhao, Bo Wei, Shuyan Li, Kongfa Chen, Na Ai, Wenhui Su

, Journal of Physics and Chemistry of Solids 70 (2009) 164.

20. H. Tsukuda, A. Notomi, N. Hisatome, J Therm Spray Technol, 9 (2000) 364.

21. Li. CJ, A. Ohmori, J Therm Spray Technol, 11 (2002) 365.

22. R. Zheng, X.M. Zhou, S.R. Wang, T.-L. Wen, C.X. Ding, J. power sources, 140 (2005) 217.

23. D. Hathiramani, R. Vaben, D. Stöver, R.J. Damani, J Therm Spray Technol, 15 (4) (2006) 593.

24. Y.S. Lin, L.G.J. De Haart, K.J. De Vries, A.J. Burggraaf. S.C. Singhal (Ed.), Proceedings of the First International Symposium on SOFCs, Hollywood, FL, The Electrochemical Society, Pennington, NJ., (1989) 67.

25. M. Lang, R. Henne, S. Schaper, G. Schiller. J. Thermal Spray Technol. 10 (4) (2001) 618.

26. S. Takenoiri, N. Kadokawa, K. Koseki, J. Thermal Spray Technol., 9 (3) (2000) 360.

27. Amel Benyoucef, Didier Klein, Christian Coddet, Boumediene Benyoucef, Development and characterisation of (Ni, Cu, Co)-YSZ and Cu-Co-YSZ cermets anode materials for SOFC application, Surface and Coatings Technology, 202 (2008) 2202.

28. A. A. Kulkarni, S. Sampath, A. Goland, H. Herman, A. J. Allen, J. Ilavsky, W. Gong and S. Gopalan, Topics in Catalysis 32 (2005) 241.

29. K.A. Khor, X.J. Chen, S.H. Chan, L.G. Yu, Microstructure-property modifications in plasma sprayed 20 wt.% yttria stabilized zirconia electrolyte by spark plasma sintering (SPS) technique, Materials Science and Engineering, 366(2004) 120.

30. Bo Liang, Hanlin Liao, Chuanxian Ding, Christian Coddet, Nanostructured zirconia–30 vol.% alumina composite coatings deposited by atmospheric plasma spraying, Thin Solid Films, 484 (2005) 225.

31. C.H. Lee, H.K. Kim, H.S. Choi, H.S. Ahn, Phase transformation and bond coat oxidation behavior of plasma-sprayed zirconia thermal barrier coating, Surf. Coat. Technol., 24 (1) (2000) 1.

32. R. Mcpherson, On the formation of thermally sprayed alumina coatings J. Mater. Sci. 15 (1980) 3141.

33. N.N. Greenwood, A. Earnshaw, Chemistry of the Elements, Butterworth-Heinemann, Amsterdam (1997) 1113.

34. O. Kubaschewski, "Oxidation of Metals and Alloys", Academic Press, NY (1962).

35. P. Kofstad, "High Temperature Corrosion", Elsevier Science Publishing Co., Inc., NY (1988).

36. K. Hauffe, "Oxidation of Metals", Plenum Press, NY (1965).

37. T. Nishizawa and K. Ishida, alloy phase diagrams, vol. 3, ASM Handbook (1991).

**Figure captions:**

Fig. 1. SEM surface morphology of (a) (2:3) Ni-YSZ, (b) (1:1:1:2) Ni-Cu-Co-YSZ coatings.

Fig. 2. SEM cross-sectional microstructure of (a) (2:3) Ni-YSZ, (b) (1:1:1:2) Ni-Cu-Co-YSZ coatings.

Fig. 3. Fracture profile of (a) Cu-YSZ (2:3), (b) Co-YSZ (2:3) coatings.

Fig. 4. XRD patterns of as deposited Ni-YSZ (2:3), Cu-YSZ (2:3), Co-YSZ (2:3), Cu-Co-YSZ (0.5:1:2.5) and Ni-Cu-Co-YSZ (1:1:1:2) coatings.

Fig. 5. XRD patterns of Ni-YSZ (2:3) after heat treatments at 800°C and 1000°C.

Fig. 6. XRD patterns of Cu-YSZ (2:3) after heat treatments at 800°C and 1000°C.

Fig.7. XRD patterns of Co-YSZ (2:3) after heat treatments at 800°C and 1000°C.

Fig. 8. XRD patterns of different weight ratios (2:3), (1:1) and (3:2) Cu-YSZ cermets, after heat treatment at 800°C.

Fig. 9. TG-DSC curves for (2:3), (1:1) and (3:2) Cu-YSZ cermets at 10°C/min heating rate under $N_2$ gas flow.

Fig. 10. XRD patterns of (0.5:1:2.5) Cu-Co-YSZ cermet, after heat treatments at 800°C and 1000°C.

Fig. 11. TG-DSC curves for (0.5:1:2.5) Cu-Co-YSZ cermet at 10°C/min heating rate under $N_2$ gas flow.

Fig. 12. XRD patterns of (1:1:1:2) Ni-Cu-Co-YSZ cermet, after heat treatments at 800°C and 1000°C.

Fig. 13. TG-DSC curves for (1:1:1:2) Ni-Cu-Co-YSZ cermet at 10°C/min heating rate under $N_2$ gas flow.

**Table caption:**

Table 1: The optimized plasma spraying parameters

Table(s)

| Conditions | Parameters | Value |
|---|---|---|
| **Plasma** | Current (A) | **500** |
| | Argon flow rate (L/min) | **38** |
| | Hydrogen flow rate (L/min) | **8** |
| | Nozzle diameter (mm) | **6** |
| **Powder injection** | Ar carrying gas flow rate (L/min) | **3,4** |
| | Powder injector diameter (mm) | **1,8** |
| | Distributor plate rotate (%) | **25** |
| | Agitation (%) | **50** |
| | Injector distance (mm) | **6** |
| | Injection angle (°) | **90** |
| **Spraying** | Spraying distance (mm) | **150** |

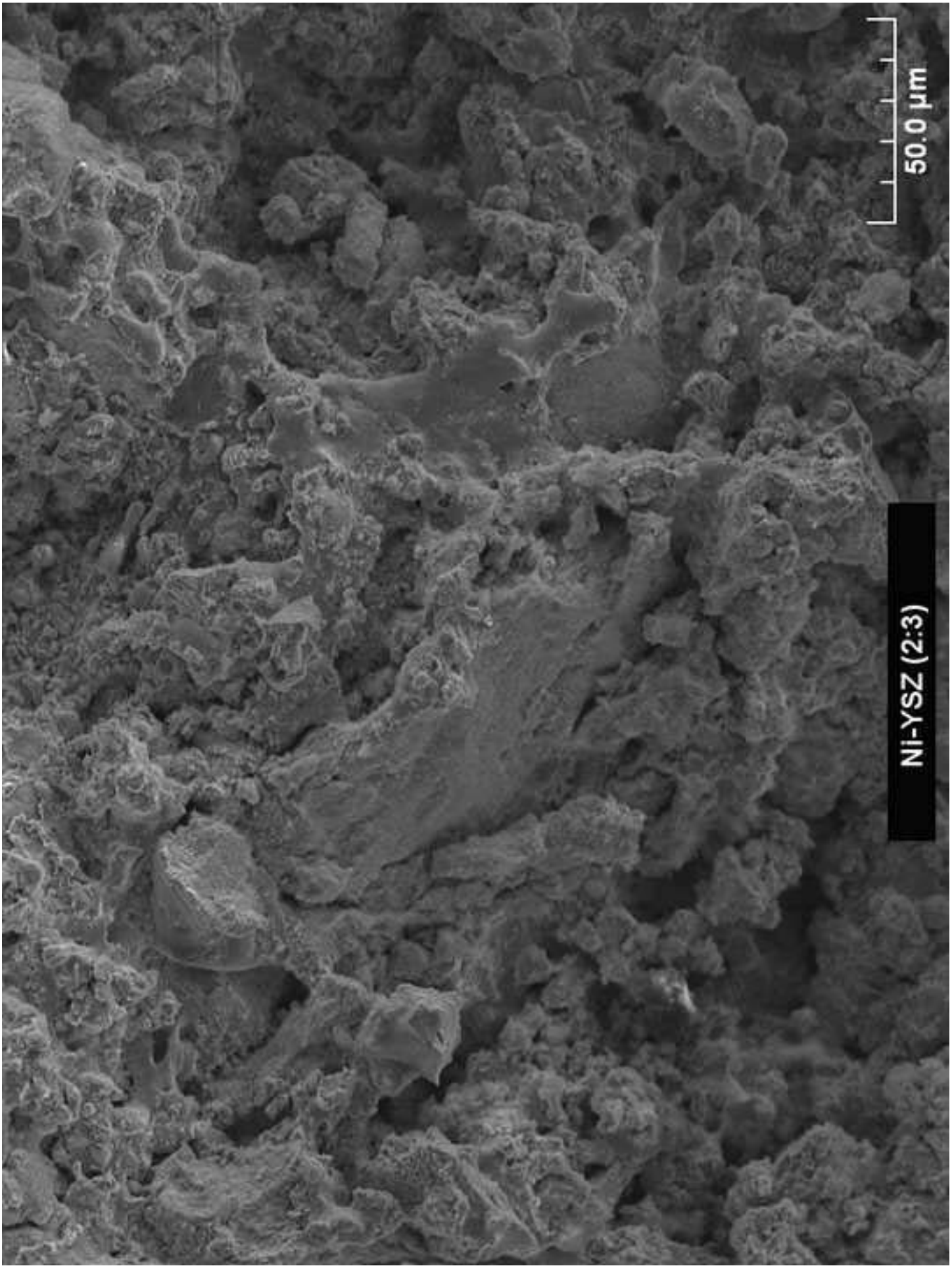


Figure(s)

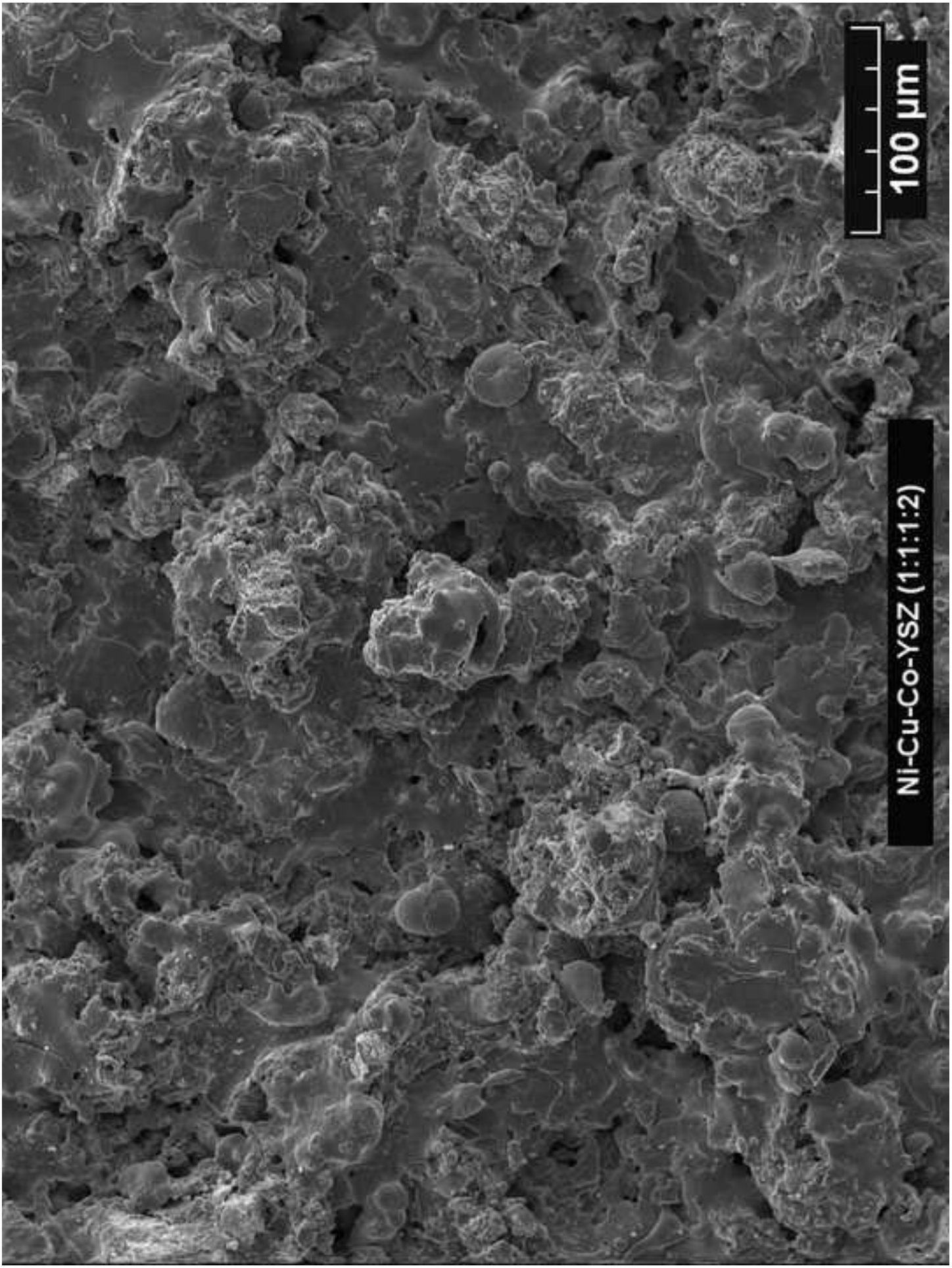


Figure(s)

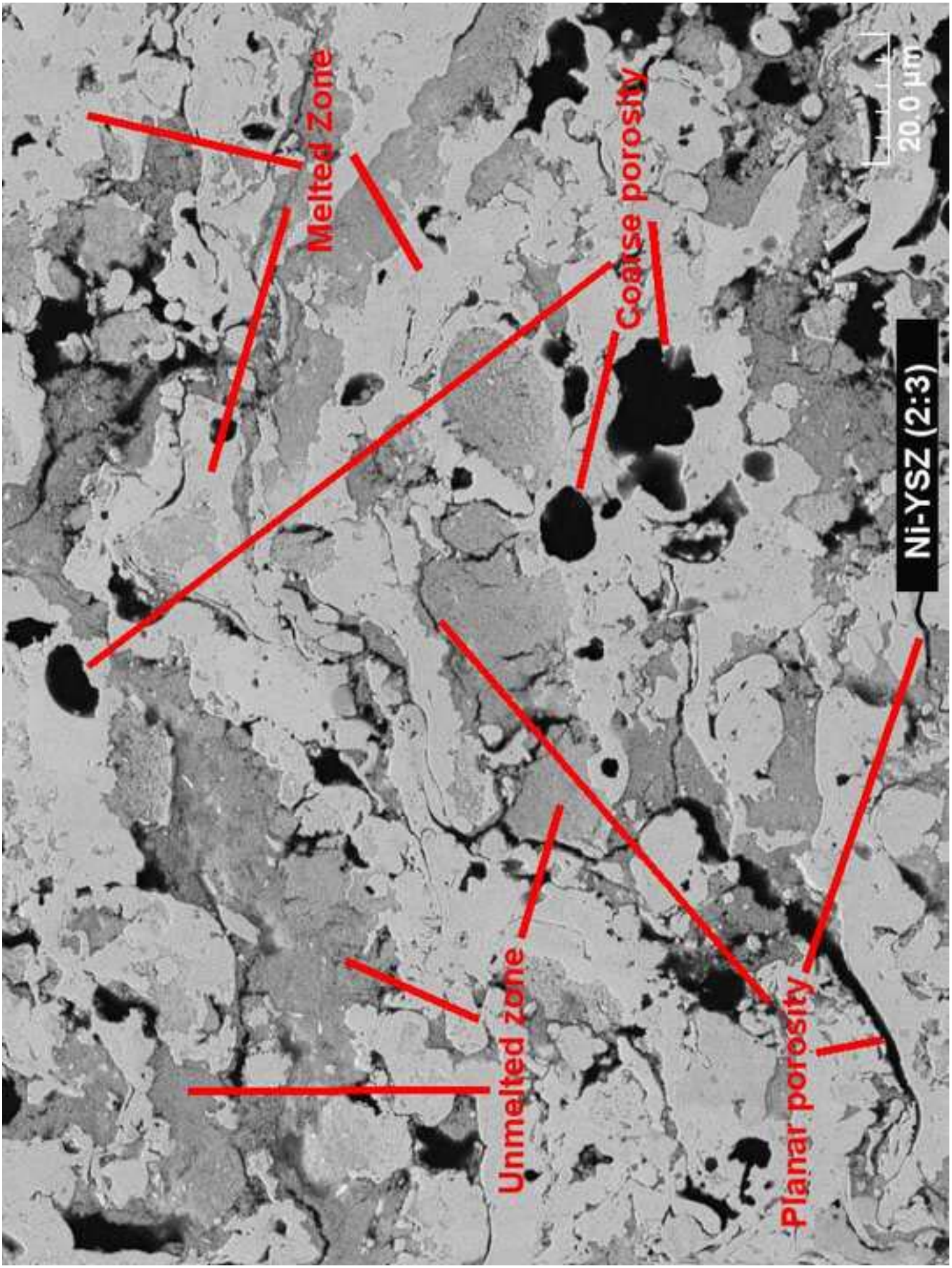


Figure(s)

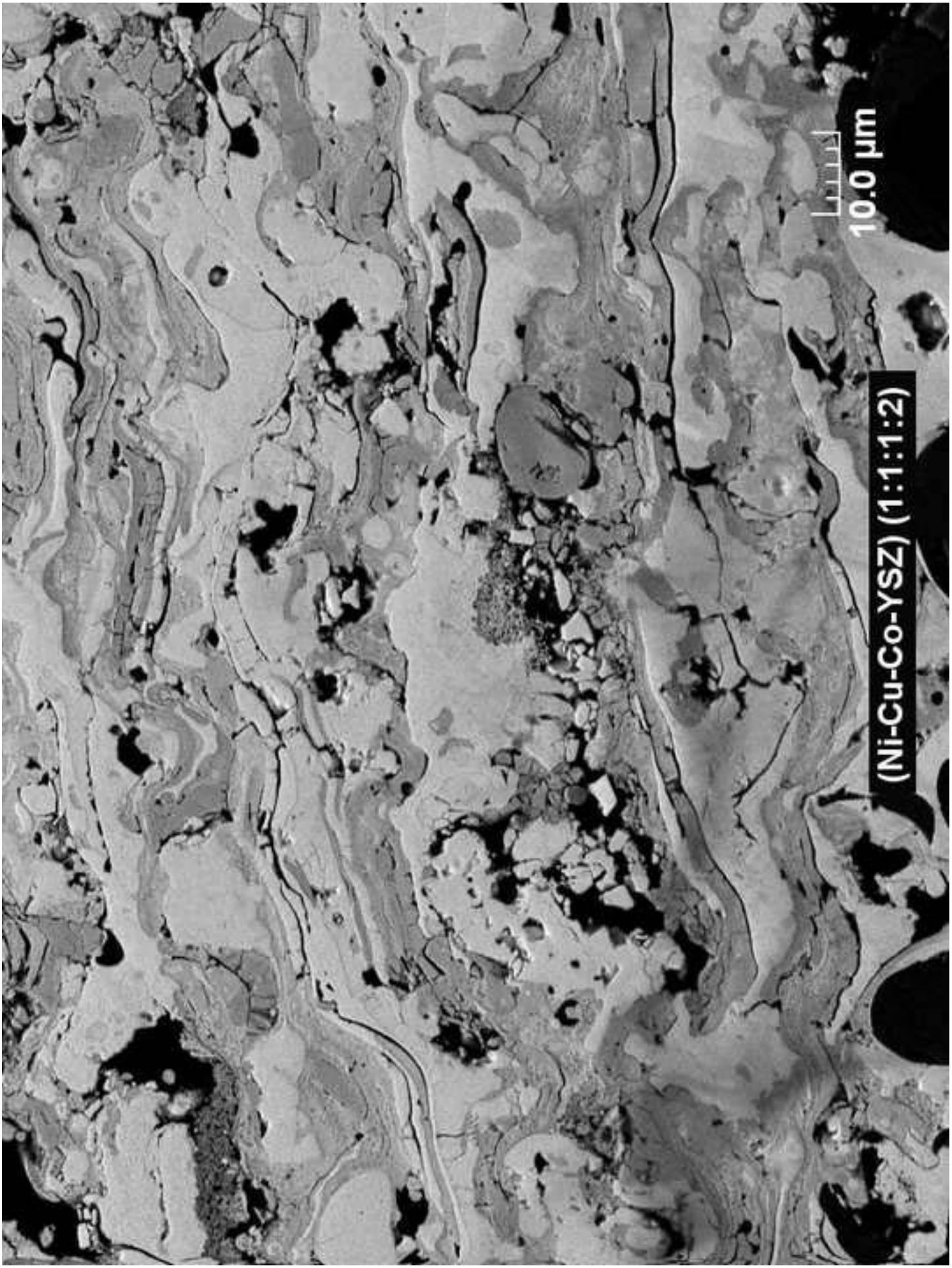


Figure(s)

Figure(s)

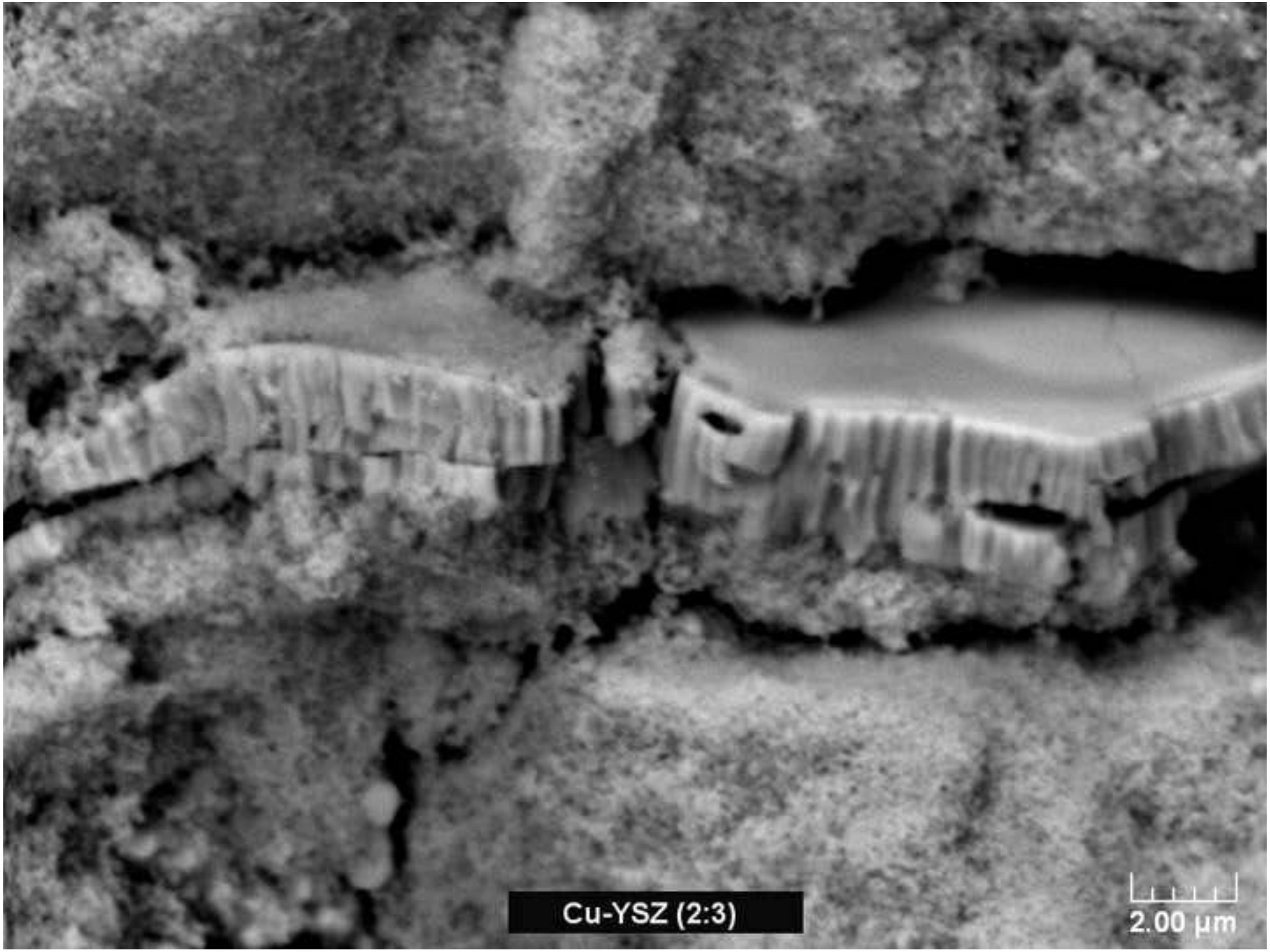

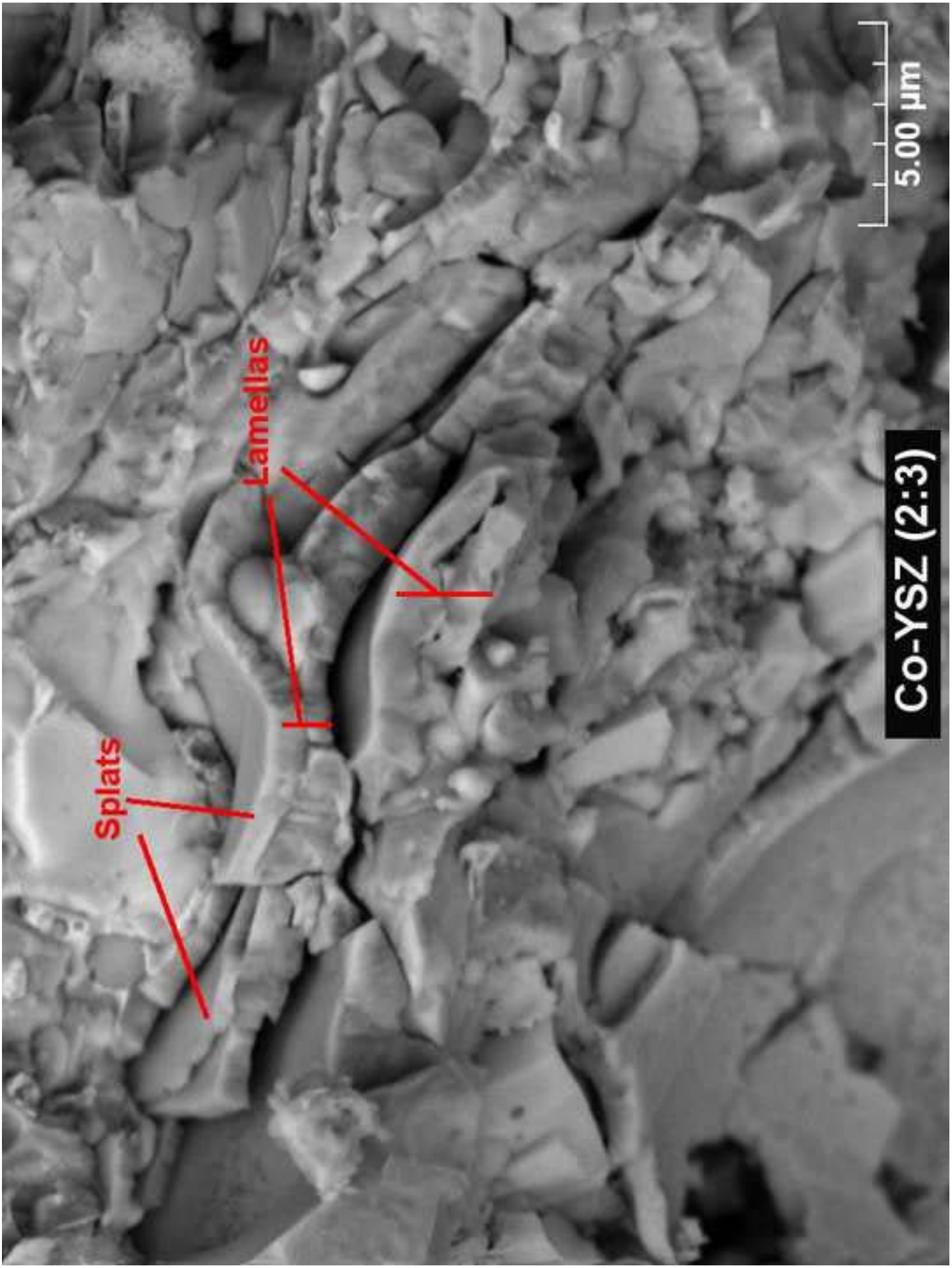


Figure(s)

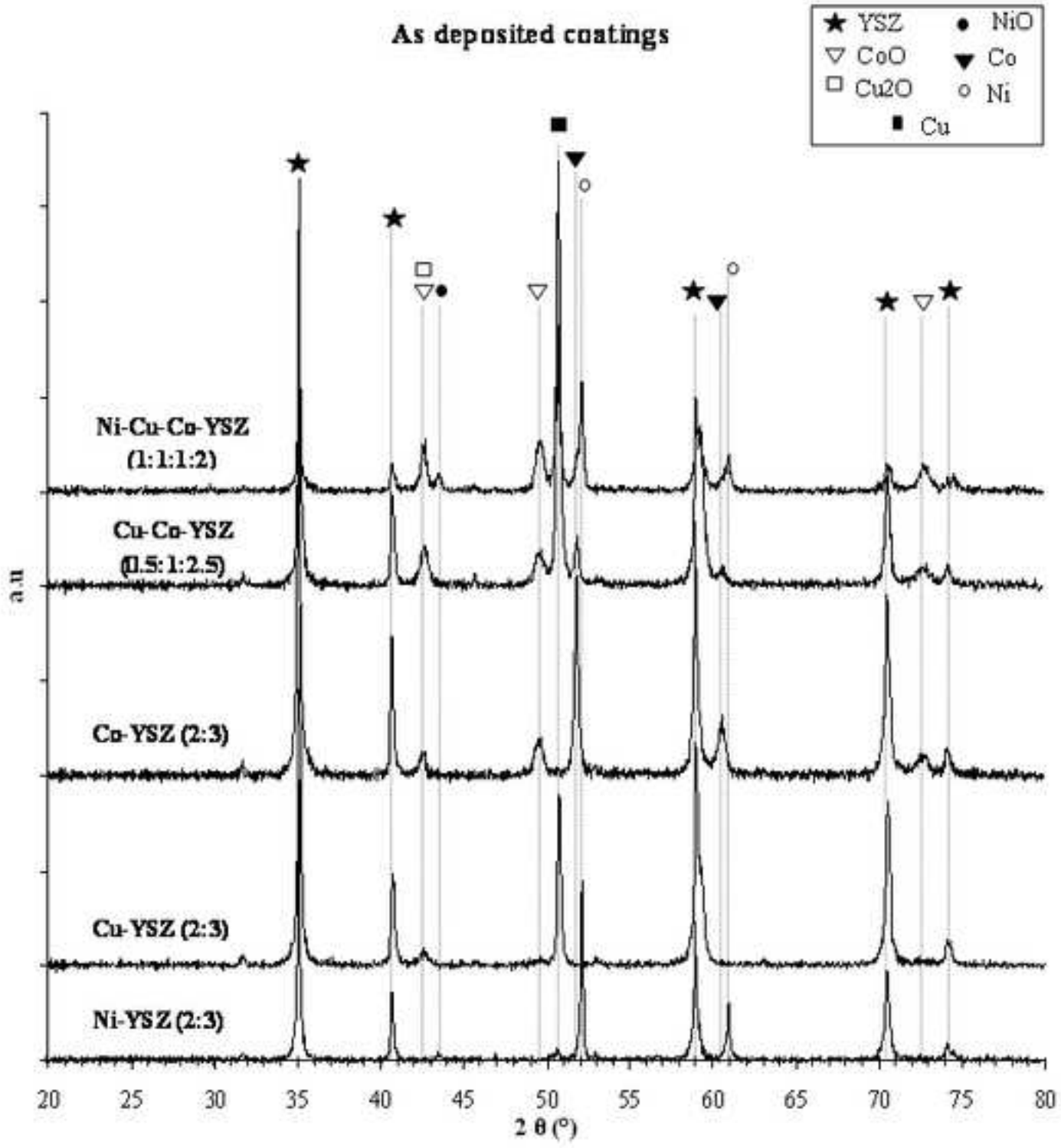

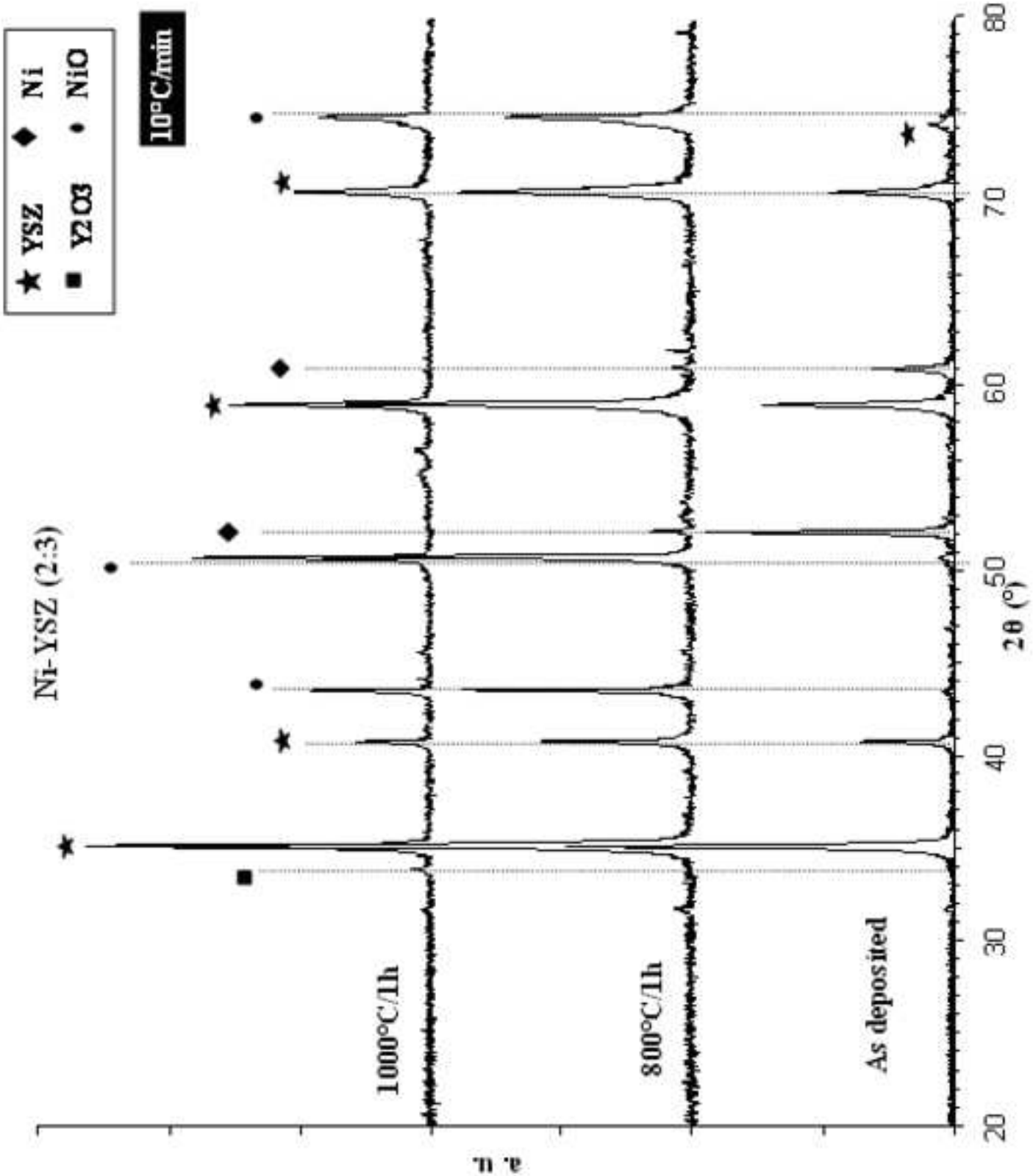


Figure(s)

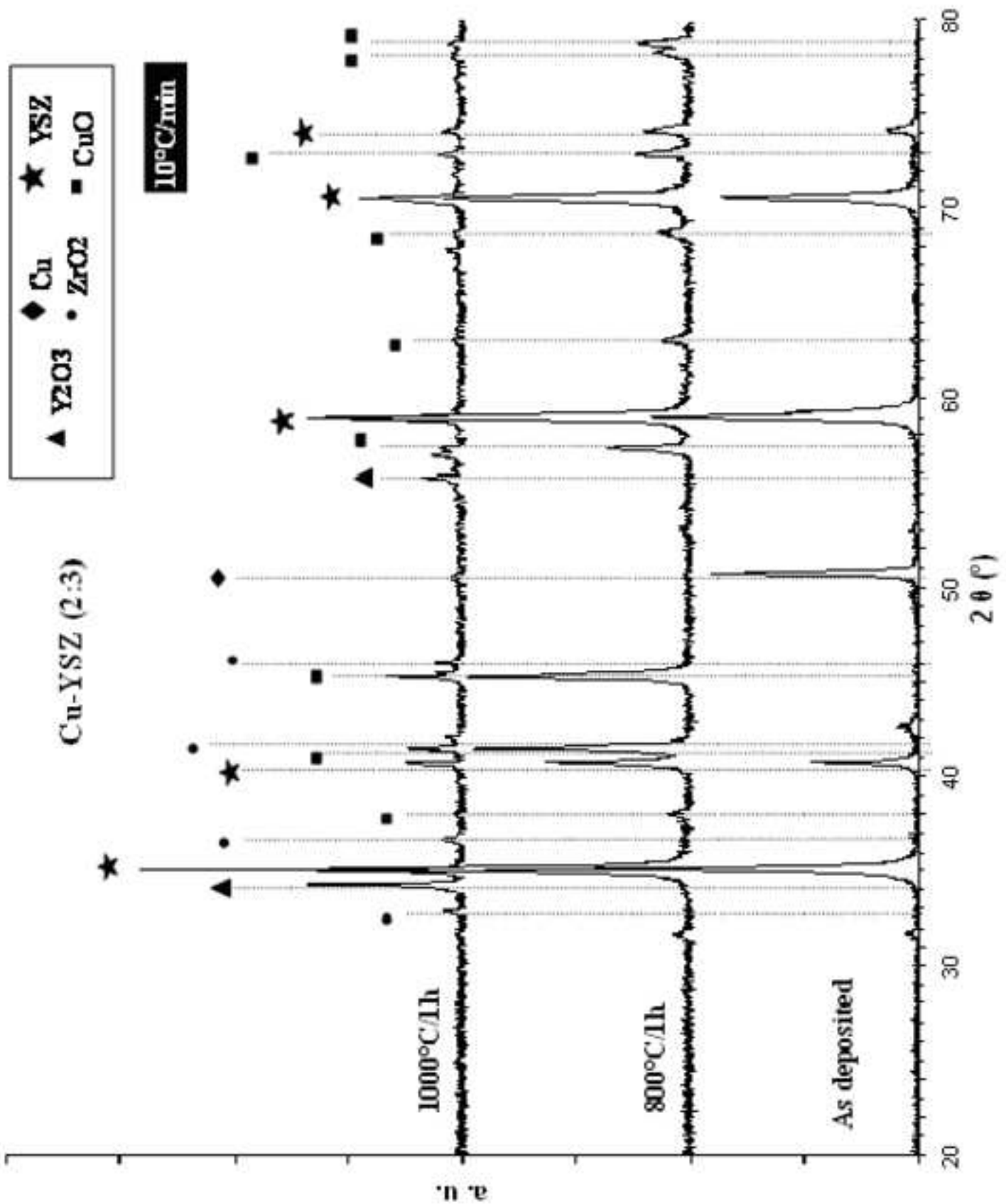


Figure(s)

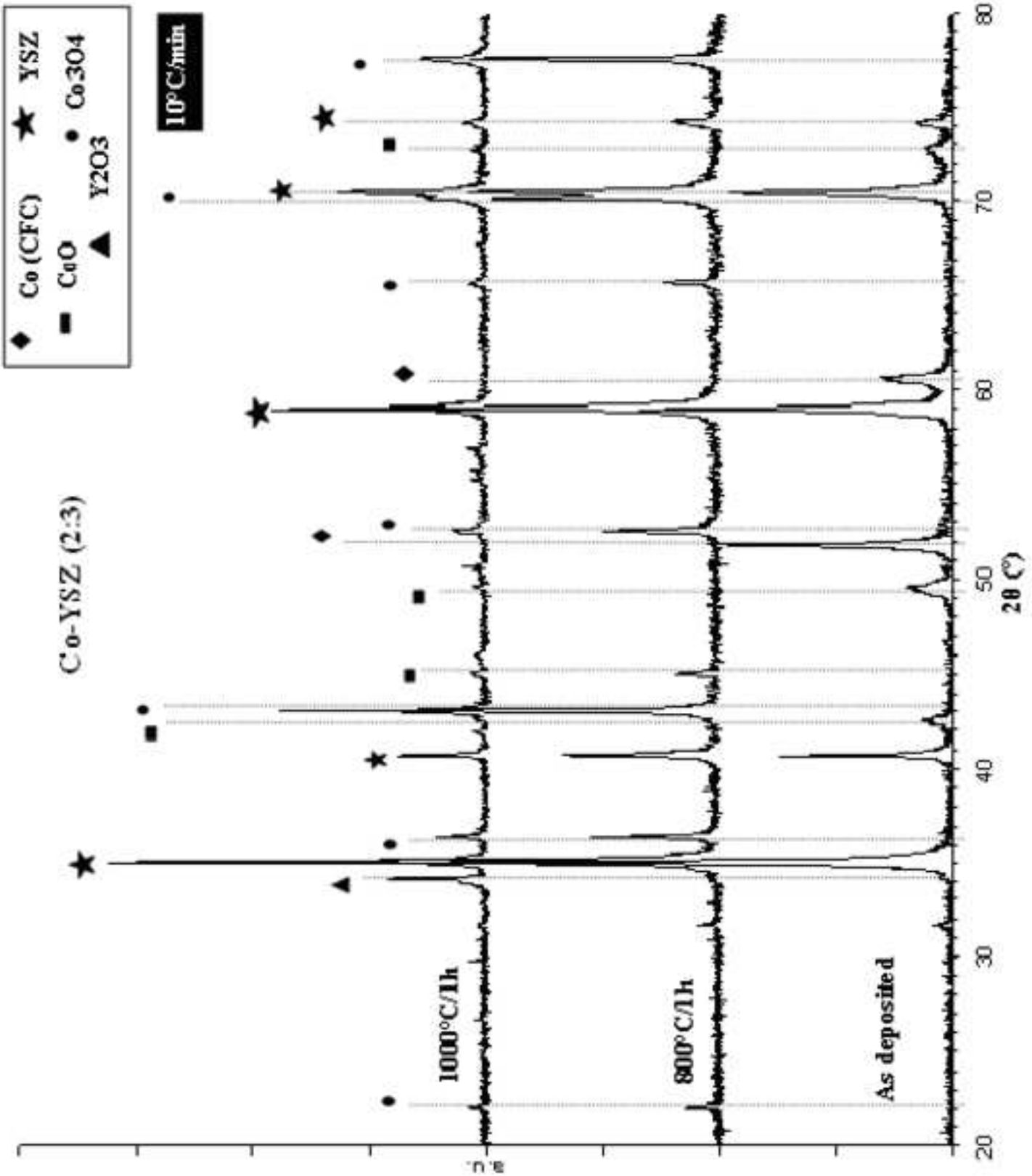


Figure(s)

Figure(s)

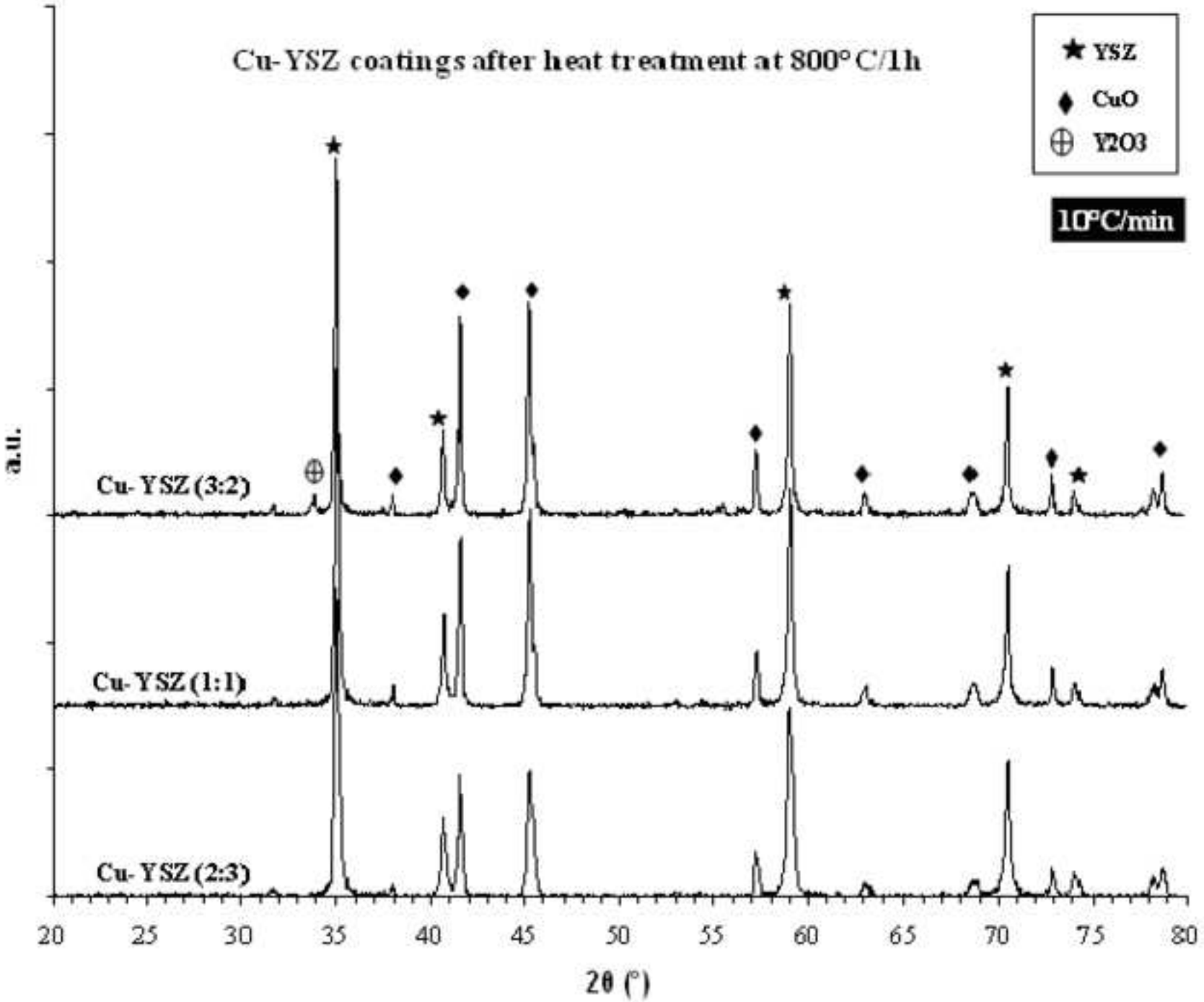

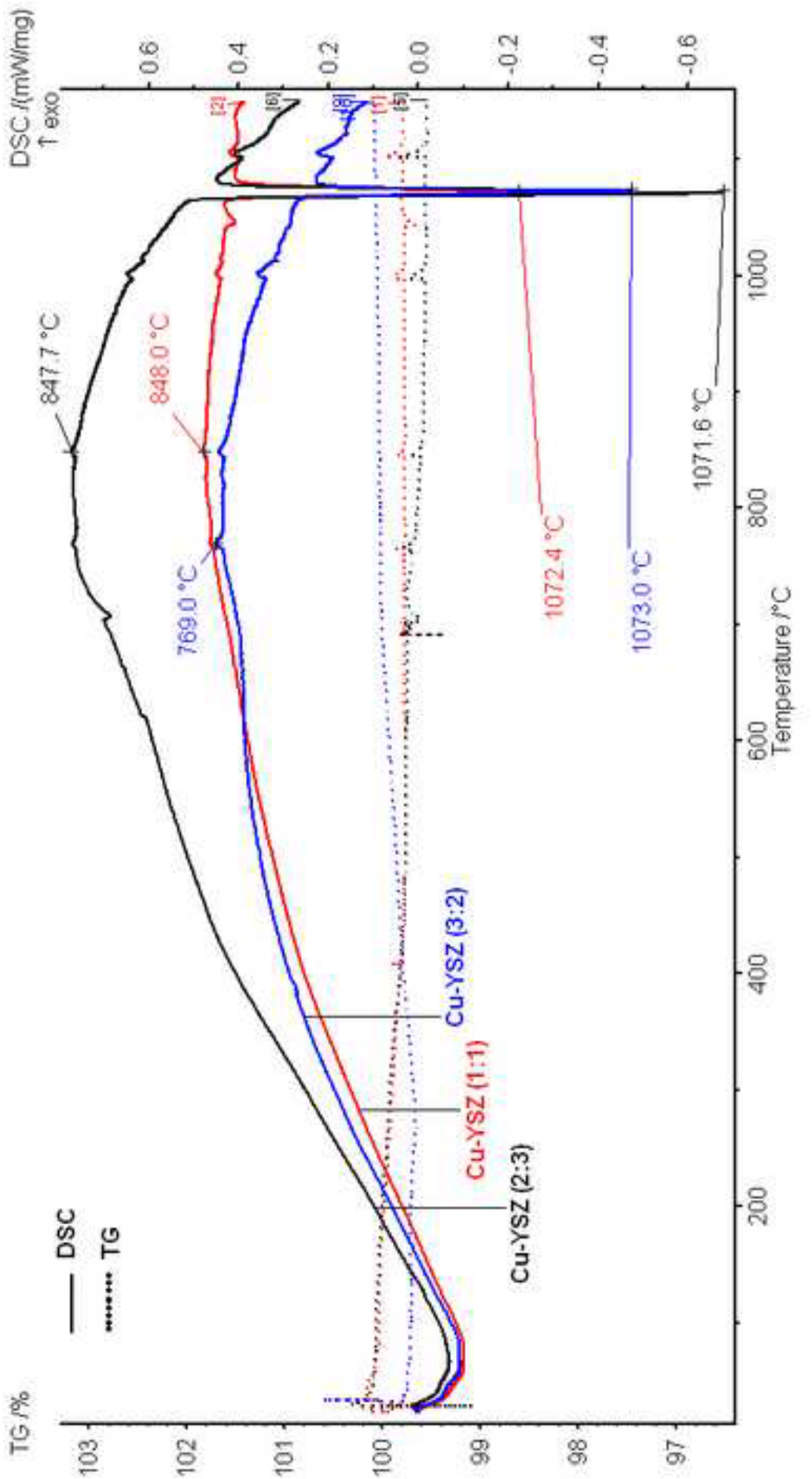


Figure(s)

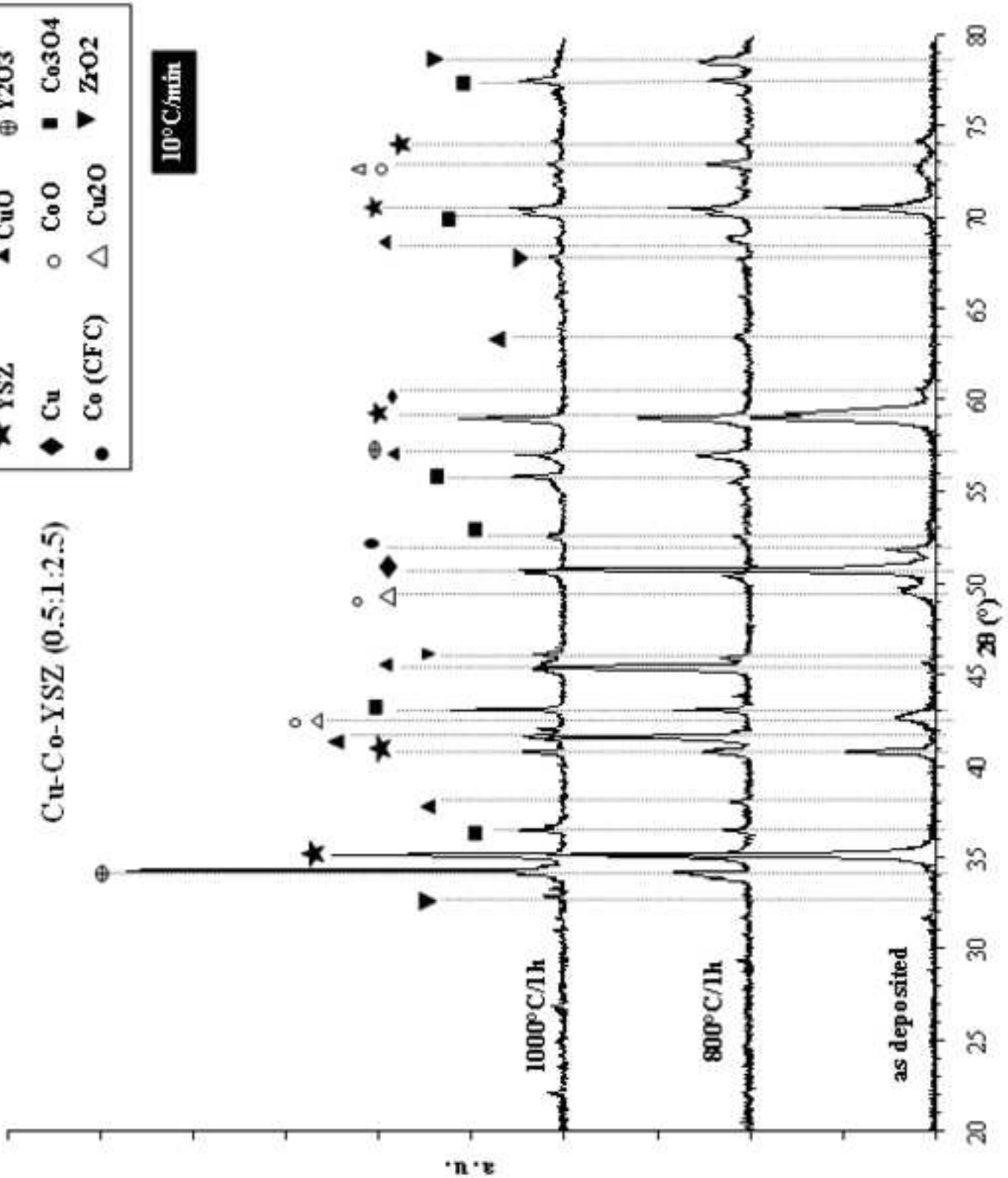


Figure(s)

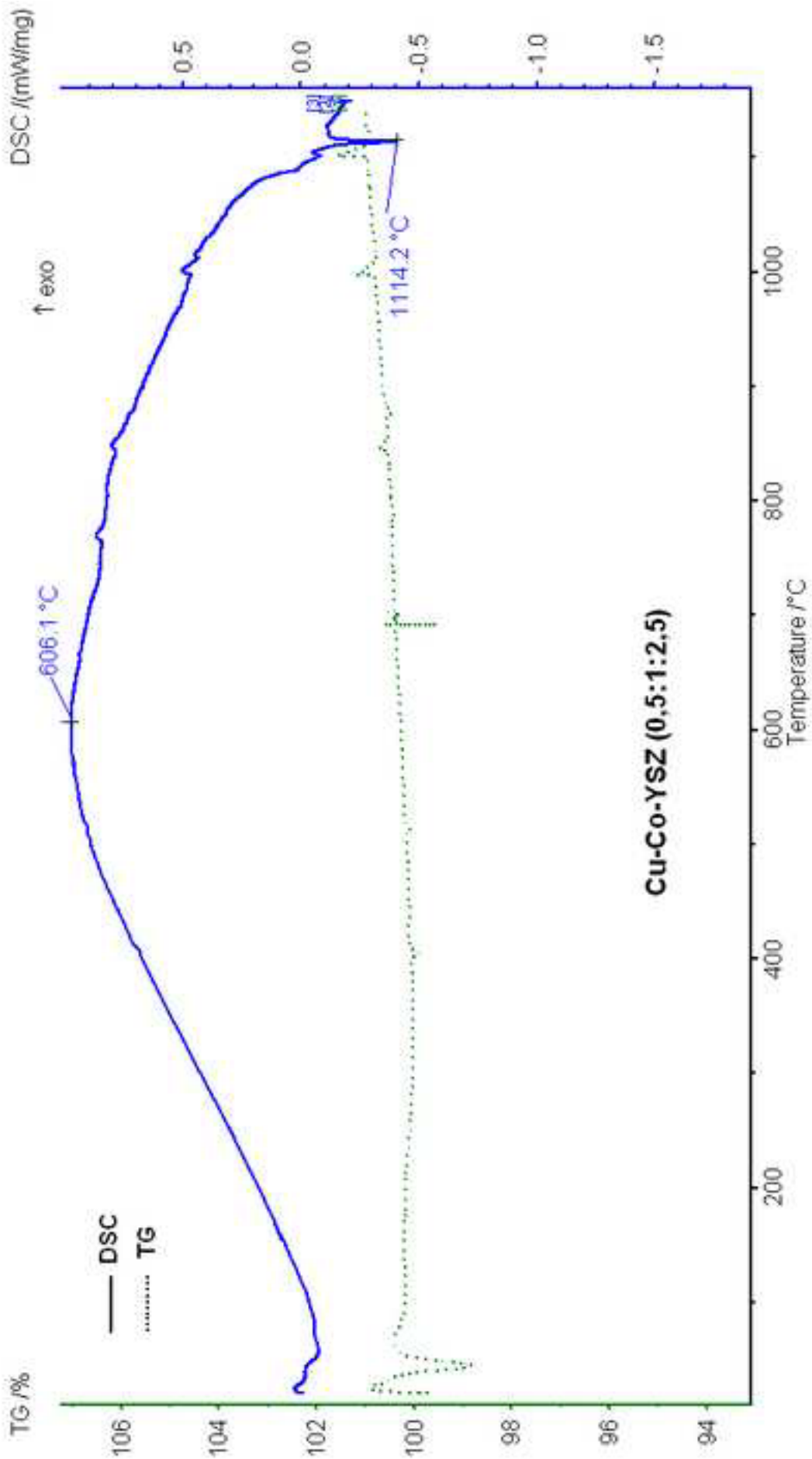


Figure(s)

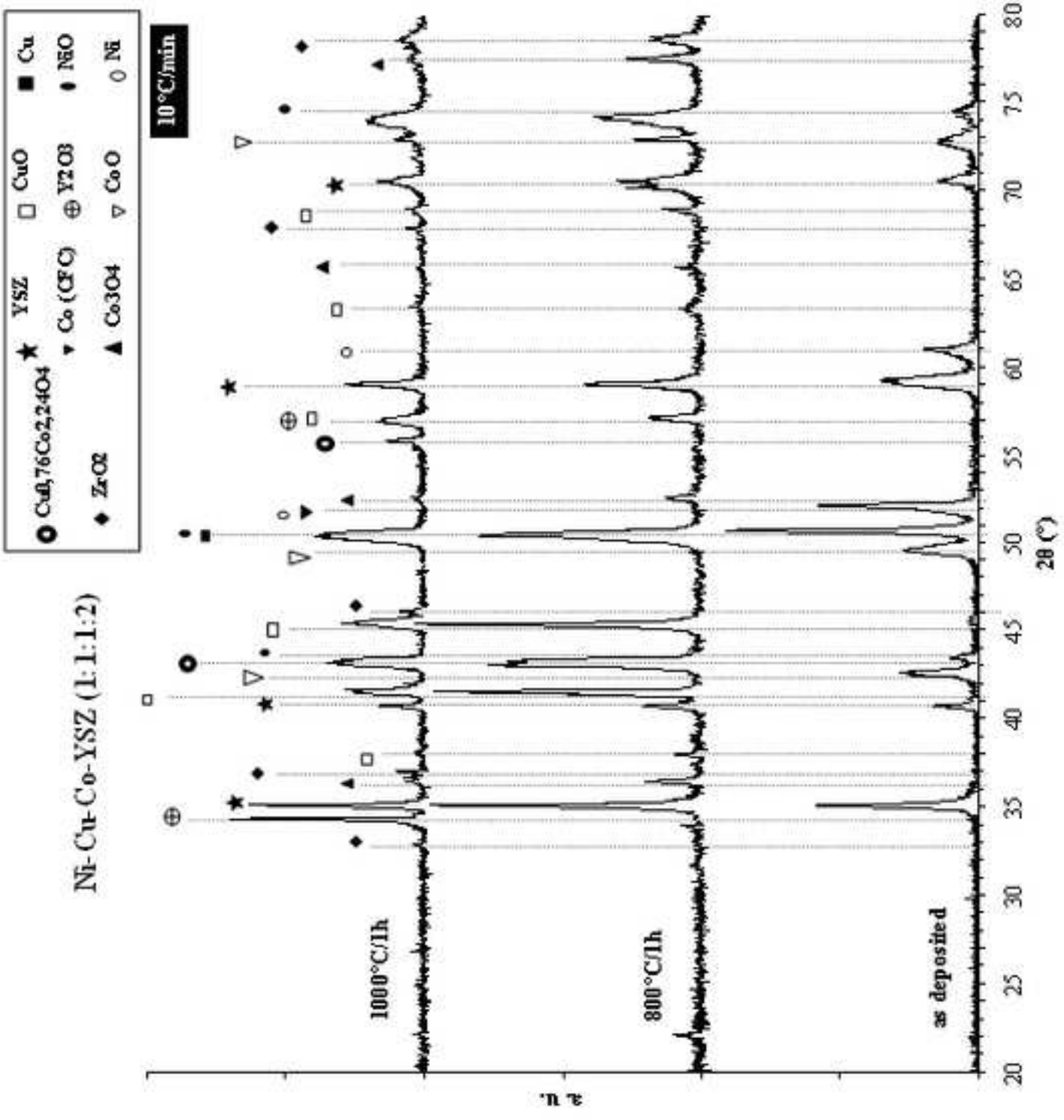


Figure(s)

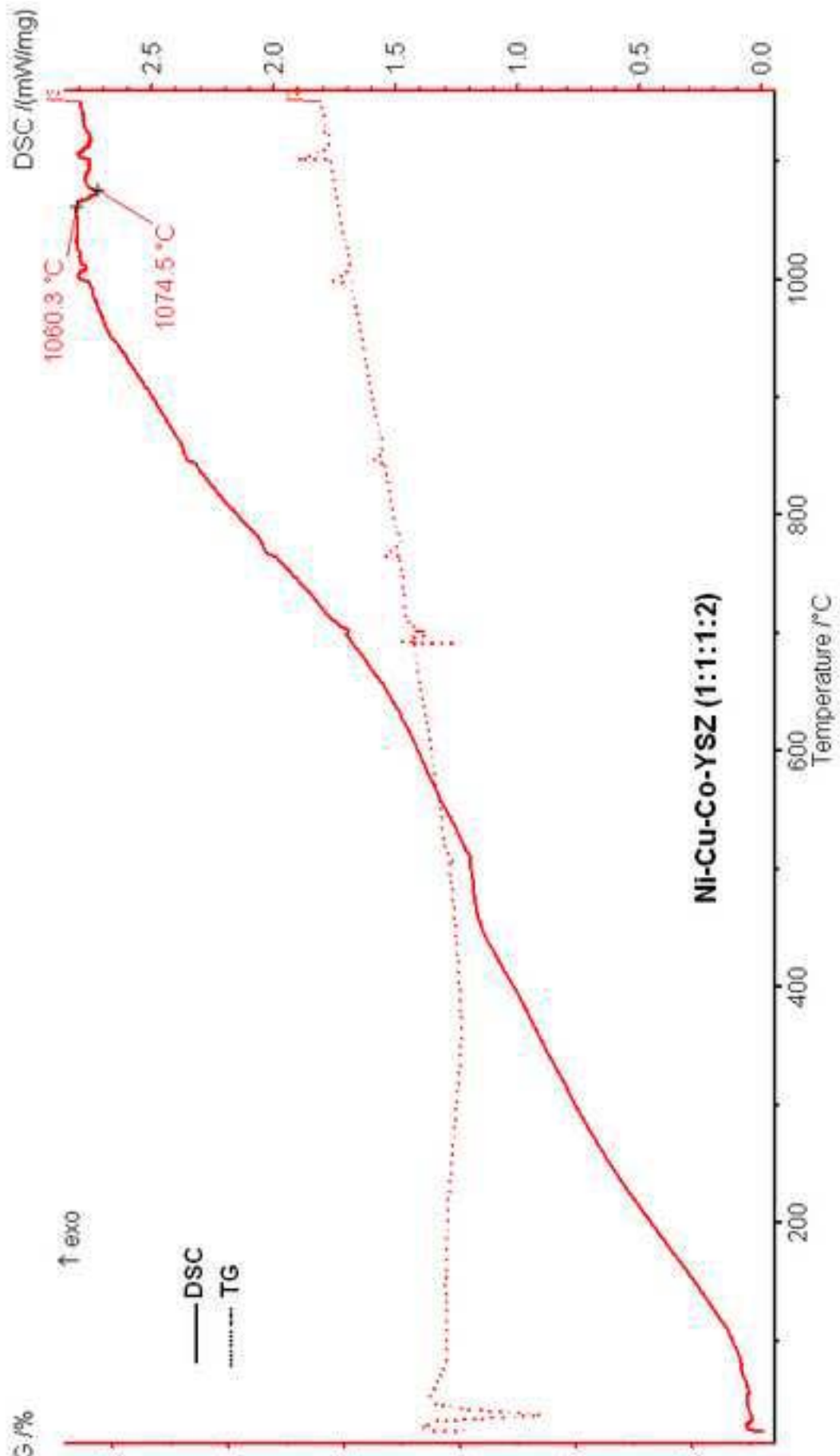


Figure(s)